

ENDMEMBER CONSTRAINT NON-NEGATIVE TENSOR FACTORIZATION VIA TOTAL VARIATION FOR HYPERSPECTRAL UNMIXING

Jin-Ju Wang, Ding-Cheng Wang, Ting-Zhu Huang*, Jie Huang*.

School of Mathematical Sciences, University of Electronic Science and Technology of China, Chengdu, Sichuan, 611731, PR China.

ABSTRACT

Hyperspectral unmixing (HU), estimating endmembers and the corresponding abundances, is crucial for the development of hyperspectral images (HSIs). To improve the unmixing performance, various spatial regularizers are imposed on the abundance matrix. Note that endmember information is also important for HU, especially when the spectral signature in HSIs are highly correlated. In this paper, we investigate information from both endmembers and abundances and propose an endmember constraint non-negative tensor factorization via total variation (EC-NTF-TV) for HU. For estimating endmembers, we introduce an endmember constraint to alleviate the spectral signatures' high correlation. In addition, we adopt the TV regularization to exploit the spatial correlation in abundance maps. Finally, we solve the proposed model under the augmented multiplicative update framework. Both synthetic and real hyperspectral data experiments demonstrate the effectiveness of the proposed algorithm.

Key words: Hyperspectral unmixing, endmember constraint, non-negative tensor factorization.

1. INTRODUCTION

Hyperspectral images (HSIs) with a large amount of spectral information are widely applied in target detection and classification, and so on. However, mixed pixels containing several pure substances (endmembers) in the low-resolution HSIs limit the development of the HSIs. Therefore, hyperspectral unmixing (HU), decomposing a mixed pixel into several endmembers and its corresponding fractions (abundances), is important for the HSIs processing [1].

A linear mixing model (LMM) is a popular way to account for the mixing process. It decomposes a mixed pixel as a linear combination of the endmembers, proportioned by their corresponding abundances [2]. Based on the LMM, non-negative matrix factorization (NMF) could simultaneously estimate endmembers and abundances [3,4]. NMF decomposes

This research is supported in part by NSFC under Grant 61772003, in part by Key Projects of Applied Basic Research in Sichuan Province under Grant 2020YJ0216, in part by National Key Research and Development Program of China under Grant 2020YFA0714001, and in part by the Fundamental Research Funds for the Central Universities under Grant ZYGX2019J093. Corresponding authors: T.-Z. Huang with tingzhuhuang@126.com; J. Huang with huangjie_uestc@uestc.edu.cn.

an HSI into a 2-D non-negative matrix represented by the endmember matrix and the abundance matrix. However, reshaping an HSI into a matrix in NMF is unavoidable to cause information loss in the horizontal direction [5, 6]. Thus, Qian et al. extend the NMF into a tensor-based model and propose a matrix-vector non-negative tensor factorization (MV-NTF) unmixing method [5]. They view an HSI as the sum of several tensors, whose number is equal to the number of endmembers. And each tensor is represented by the outer product of a matrix (abundance map) and a vector (endmember signature).

Due to the non-convexity of NMF and MV-NTF, various regularizers are considered to obtain stable solutions. In [4], Qian et.al introduce an $\ell_{1/2}$ norm to enhance the sparsity of the abundance matrix. To suppress the noise, a total variation (TV) regularized MV-NTF method is proposed in [6]. These methods have achieved promising unmixing results.

Considering the high correlation of spectral curves in the HSIs, in this paper, we propose an algorithm named endmember constrained non-negative tensor factorization via total variation (EC-NTF-TV) for hyperspectral unmixing. It alleviates the high correlation among spectral signatures from aspects of the endmembers and the abundance maps. For the endmembers, we introduce an endmember constraint to remain the feature of each endmember and keep it to be smooth. For the abundance maps, we adopt the TV regularization to exploit the piece-wise smoothness of the HSIs. Then, we adopt the augmented multiplicative algorithm to solve the proposed model. Experiments on both synthetic and real data have shown our method outperforms several state-of-the-art approaches.

2. BASIC UNMIXING MODEL

Given an HSI with $I \times J$ pixels and K bands, $\mathcal{Y} \in \mathbb{R}^{I \times J \times K}$, then we reshape the 3-D HSI to a matrix $\mathbf{Y} \in \mathbb{R}^{K \times IJ}$. Then, the unmixing model based on the LMM is

$$\mathbf{Y} = \mathbf{C}\mathbf{X} + \mathbf{N}, \quad (1)$$

where $\mathbf{C} \in \mathbb{R}^{K \times R}$ is the endmember matrix containing R endmembers, $\mathbf{X} \in \mathbb{R}^{R \times IJ}$ represents the abundance matrix, and \mathbf{N} represents the additive white Gaussian noise.

In MV-NTF [5], the 3-D HSI is represented as the sum of some tensors, which is the outer product of the endmembers

and their corresponding abundance maps. By the definition of the abundances, the abundance matrix meets two conditions: the abundance non-negativity constraint (ANC, i.e., $\mathbf{X} \geq \mathbf{0}$) and the abundance sum-to-one constraint (ASC, i.e., $\mathbf{1}_R^T \mathbf{X} = \mathbf{1}_{I,J}^T$) [2]. Based on the LMM, the MV-NTF model is

$$\begin{aligned} \mathcal{Y} &= \sum_{r=1}^R \mathbf{E}_r \circ \mathbf{c}_r + \mathcal{N} = \sum_{r=1}^R \mathbf{A}_r \mathbf{B}_r^T \circ \mathbf{c}_r + \mathcal{N}, \\ \text{s.t. } \mathbf{E}_1 + \cdots + \mathbf{E}_R &= \mathbf{1}_{I \times J}, \end{aligned} \quad (2)$$

where \circ is the outer product [7], and $\mathbf{1}_{I \times J} \in \mathbb{R}^{I \times J}$ is the matrix with all elements are 1. In (2), $\mathbf{E}_r \in \mathbb{R}^{I \times J}$ is the abundance map corresponding to the r -th endmember \mathbf{c}_r in \mathbf{C} . Each abundance map \mathbf{E}_r is represented by the product of two low-rank matrices $\mathbf{A}_r \in \mathbb{R}^{I \times L_r}$ and $\mathbf{B}_r \in \mathbb{R}^{J \times L_r}$ to describe the low-rankness property.

3. THE PROPOSED EC-NTF-TV ALGORITHM

To alleviate the high correlation of spectral curves in the HSIs, we simultaneously exploit the information from the endmembers and the abundance maps. Thus, in this section, we first introduce the proposed endmember constraint and then propose the EC-NTF-TV algorithm.

1) Endmember Constraint: In practice, spectral curves in HSIs are highly correlated [8]. In this case, only exploiting spatial information is hard to separate the spectral curves adequately. Thus, we introduce a new endmember constraint, which aims to catch the endmember's features and keep them to be smooth. Recall that the bilateral filter is a popular image processing technique, which simultaneously preserves the edge and smooths the homogeneous region [9]. Based on BF, the endmember constraint is as follows

$$g(\mathbf{C}) = \|\mathbf{C} \cdot * \mathbf{W}\|_F^2, \quad (3)$$

where $\cdot *$ denotes the element-wise product. Here, $\mathbf{W} = [\mathbf{w}_1, \dots, \mathbf{w}_R]$ is a weighting matrix, its i -th column $\mathbf{w}_i = 1. / (\text{BF}(\mathbf{c}_i) + \eta)$, $i = 1, \dots, R$, where BF is the bilateral filter, $./$ denotes the element-wise division, and η is a small value.

2) Model and Algorithm: For the abundance maps, we use the TV regularization to investigate the piece-wise smoothness of the HSIs. Under the framework of the NTF, we formulate our objective function as

$$\begin{aligned} \mathcal{L}(\mathbf{E}, \mathbf{C}, \mathbf{U}) &= \frac{1}{2} \|\mathcal{Y} - \sum_{r=1}^R \mathbf{E}_r \circ \mathbf{c}_r\|_F^2 + \frac{\delta}{2} \|\mathbf{1}_{I \times J} - \mathbf{E} \mathbf{D}^T\|_F^2 \\ &\quad + \frac{\lambda_1}{2} \|\mathbf{C} \cdot * \mathbf{W}\|_F^2 + \lambda_2 \sum_{r=1}^R (\mathbf{E}_r)_{TV} + \frac{\mu}{2} \|\mathbf{E} - \mathbf{U}\|_F^2 \\ &\quad + \text{Tr}(\mathbf{T}\mathbf{E}) + \text{Tr}(\Phi\mathbf{C}), \end{aligned} \quad (4)$$

where $\mathbf{E} = [\mathbf{E}_1, \dots, \mathbf{E}_R]$, $\mathbf{C} = [\mathbf{c}_1, \dots, \mathbf{c}_R]$, $\mathbf{D} = [\mathbf{D}_1, \dots, \mathbf{D}_R]$, \mathbf{I}_n is an identity matrix. In (4),

Γ and Φ are Lagrange multipliers for each non-negative variable in (4), and $\mu > 0$ is a penalty parameter. Similarly as in [10], we solve (4) using the augmented multiplicative algorithm.

For the \mathbf{E} -subproblem, we solve the following problem

$$\min_{\mathbf{E}} \frac{1}{2} \|\mathbf{Y}_{(1)} - \mathbf{M}_1 \mathbf{E}^T\|_F^2 + \frac{\delta}{2} \|\mathbf{1}_{I \times J} - \mathbf{E} \mathbf{D}^T\|_F^2 + \frac{\mu}{2} \|\mathbf{E} - \mathbf{U}\|_F^2,$$

where $\mathbf{Y}_{(1)}$ is the mode-1 unfolding of \mathcal{Y} . And $\mathbf{M}_1 = \mathbf{D} \bar{\odot} \mathbf{C}$, where $\bar{\odot}$ is the generalized Khatri-Rao product [7]. And the update rule for \mathbf{E} is obtained

$$\begin{aligned} \mathbf{E}^{(t+1)} &= \mathbf{E}^{(t)} \cdot * (\mathbf{Y}_{(1)}^T \mathbf{M}_1 + \delta \mathbf{1}_{I \times J} \mathbf{D} + \mu \mathbf{U}) \\ &\quad ./ (\delta \mathbf{E}^{(t)} \mathbf{D}^T \mathbf{D} + \mathbf{E}^{(t)} \mathbf{M}_1^T \mathbf{M}_1 + \mu \mathbf{E}^{(t)}). \end{aligned} \quad (5)$$

Similarly as in the \mathbf{E} -subproblem, the solution of the \mathbf{C} -subproblem is obtained by

$$\mathbf{C}^{(t+1)} = \mathbf{C}^{(t)} \cdot * (\mathbf{Y}_{(3)}^T \mathbf{M}_2) ./ (\mathbf{C}^{(t)} \mathbf{M}_2^T \mathbf{M}_2 + \lambda_1 \mathbf{C}^{(t)} \mathbf{W}^{(t)}), \quad (6)$$

where $\mathbf{Y}_{(3)}$ is the mode-3 unfoldings of \mathcal{Y} . And $\mathbf{M}_2 = [(\mathbf{E}_1 \odot \mathbf{D}_1) \mathbf{1}_L \cdots (\mathbf{E}_R \odot \mathbf{D}_R) \mathbf{1}_L]$, where \odot is the Khatri-Rao product [7]. In (6), $\mathbf{W}^{(t)} = [\mathbf{w}_1^{(t)}, \dots, \mathbf{w}_R^{(t)}]$, $\mathbf{w}_i^{(t)}$ is the i -th column in $\mathbf{W}^{(t)}$. And $\mathbf{w}_i^{(t)} = 1. / (\text{BF}(\mathbf{c}_i^{(t-1)}) + \eta)$, where η is small value, $\mathbf{c}_i^{(t-1)}$ is the i -th column in $\mathbf{C}^{(t-1)}$, and $./$ denotes element-wise division.

To solve \mathbf{U} -subproblem, we divide it into R subproblems

$$\mathbf{U}_r^{(t+1)} = \underset{\mathbf{U}_r}{\operatorname{argmin}} \frac{\mu}{2} \|\mathbf{E}_r - \mathbf{U}_r\|_F^2 + \lambda_2 (\mathbf{U}_r)_{TV}. \quad (7)$$

We solve (7) by using fast gradient projection (FGP) algorithm in [11]. According to the above analysis, we summarize the corresponding algorithm in Algorithm 1. According to Algorithm 1, we can obtain that the computational complexity of EC-NTF-TV is $\mathbf{O}(IJ^2R^2L + ILR^2J^3 + IJLR^2)$.

Algorithm 1: EC-NTF-TV.

Input: An HSI cube $\mathcal{Y} \in \mathbb{R}^{I \times J \times L}$;

The parameters $\delta, \lambda_1, \lambda_2$ and μ .

The number of endmembers R .

Initialization: $\mathbf{E}^{(0)}, \mathbf{C}^{(0)}, \mathbf{W}^{(0)}, \mathbf{U}_r^{(0)} = \mathbf{E}_r^{(0)}$ for $r = 1, \dots, R$.

Repeat:

Update $\mathbf{E}^{(t+1)}$ by (5)

Update $\mathbf{C}^{(t+1)}$ by (6)

Update $\mathbf{U}_r^{(t+1)}$ by FGP

Until termination condition is met.

4. SYNTHETIC DATA EXPERIMENTS

In this section, we compare the unmixing performance of the comparing methods with relative works: $L_{1/2}$ -NMF [4],

MV-NTF [5], and MV-NTF-TV [6], on synthetic data with 128×128 pixels and 431 bands. By LMM, five endmembers are selected and the corresponding abundance maps are shown in Fig. 2. For EC-NTF-TV, we adopt the random initialization to set $\mathbf{E}^{(0)}$ and $\mathbf{C}^{(0)}$ and we set $\delta = 0.4$, $\lambda_1 = 5$, $\lambda_2 = 0.1$, and $\mu = 0.001$. To quantitatively show the unmixing performance, we adopt the spectral angle distance (SAD) and root-mean-square error (RMSE) for endmember signatures and abundance maps. In addition, each test has been performed 10 times and average SAD and RMSE are recorded.

Table 1 shows the values of SAD and RMSE obtained by different algorithms. From Table 1, we see that our method achieves better SAD and RMSE than other methods. Figs. 1 and 2 present the estimated spectral curves and abundance maps by comparing methods on the synthetic data, respectively. From Figs. 1 and 2, our results are closer to the references than others.

Table 1. The SAD and RMSE of different algorithms on the synthetic data.

Algorithm	SAD						RMSE
	End 1	End 2	End 3	End 4	End5	Mean	
$L_{1/2}$ -NMF	0.3522	0.2858	0.2123	0.1792	0.0961	0.2259	0.2004
MV-NTF	0.2224	0.1113	0.1259	0.1372	0.1794	0.1557	0.1763
MV-NTF-TV	0.2194	0.1356	0.1175	0.1191	0.1741	0.1511	0.1701
EC-NTF-TV	0.1645	0.1064	0.0672	0.0309	0.0808	0.0899	0.1287

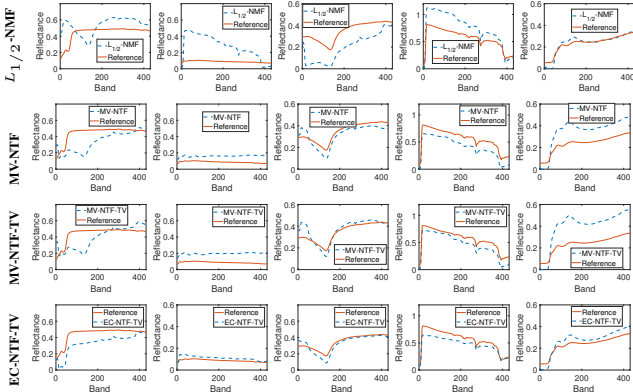


Fig. 1. References and estimated spectral curves by different unmixing algorithms on the synthetic data. From left to right: endmembers 1 to 5.

5. REAL-WORLD DATA EXPERIMENT

In this section, we use Jasper Ridge data to show the unmixing performance of the comparing methods. The Jasper Ridge data set contains 512×614 pixels with 224 bands, whose

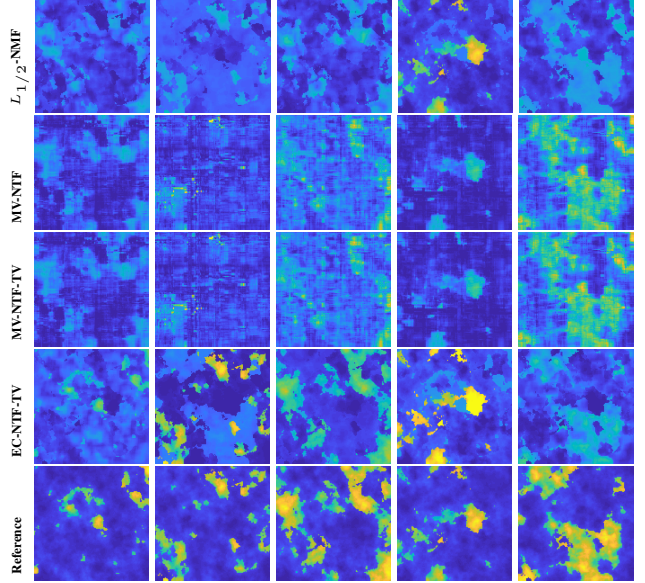


Fig. 2. References and estimated abundance maps by different unmixing algorithms on the synthetic data for endmembers 1 to 5.

reflectance value distributes uniformly ranging from 0.38 to $2.5 \mu\text{m}$. Due to the effect of water-absorption and noise, we delete bands 1-3, 108-112, 154-166, and 220-224 and leave 198 channels. In addition, we adopt a 100×100 -pixel subimage of Jasper Ridge data, which contains four endmembers: road, soil, water, and tree.

Quantitative results on the Jasper Ridge data set are shown in Table 2. From Table 2, MV-NTF-TV obtains the lower SAD for the endmember soil. For the endmembers tree, water, and road, our method's SADs are lower than others. In addition, our method achieves the best mean SAD on Jasper Ridge data set. We also show the estimated endmembers and abundances by the comparing methods on Jasper Ridge data in Figs. 3 and 4. For the spectral curves for the endmembers tree, water, and road, our results are closer to the references. As Fig. 4 shown, our method provides closer abundance maps to the references.

Table 2. The SAD of different algorithms on the Jasper Ridge data.

Algorithm	Tree	Water	Soil	Road	Mean
$L_{1/2}$ -NMF	0.2161	0.2230	0.2503	0.2349	0.2311
MV-NTF	0.2168	0.1810	0.1784	0.1588	0.1847
MV-NTF-TV	0.2007	0.2293	0.1314	0.2294	0.1977
EC-NTF-TV	0.1622	0.0711	0.1933	0.0726	0.1248

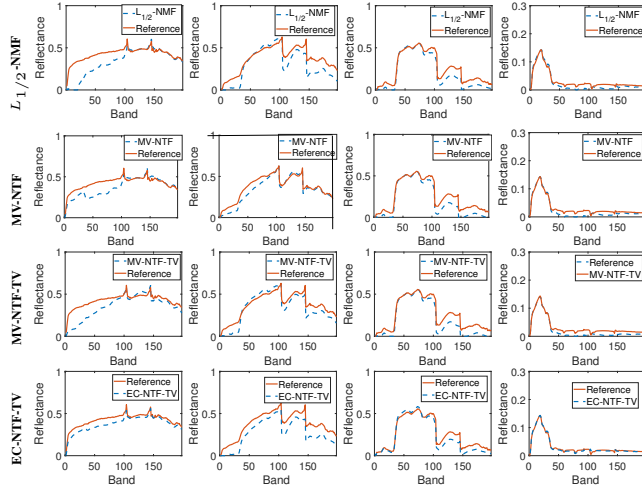


Fig. 3. References and estimated spectral curves by different unmixing algorithms for road, soil, tree, and water on Jasper Ridge data set.

6. CONCLUSIONS

In this paper, we propose an endmember constraint non-negative tensor factorization via total variation, named EC-NTF-TV, for hyperspectral unmixing. It considers information from both endmembers and abundances to alleviate the spectral signatures' high correlation. Specifically, we introduce an endmember constraint on endmembers and use the TV regularization to exploit the abundance map. An augmented multiplicative algorithm is adopted to obtain updated rules. Experimental results on both synthetic data and real-world data demonstrate the effectiveness of our algorithm.

7. REFERENCES

- [1] J. M. Bioucasdias, A. Plaza, N. Dobigeon, M. Parente, Q. Du, P. Q. Gader, and J. Chanussot, "Hyperspectral unmixing overview: Geometrical, statistical, and sparse regression-based approaches," *IEEE J. Sel. Topics Appl. Earth Observat. Remote Sens.*, vol. 5, no. 2, pp. 354–379, 2012.
- [2] N. Keshava and J. Mustard, "Spectral unmixing," *IEEE Signal Process. Mag.*, vol. 19, no. 1, pp. 44–57, 2002.
- [3] V. P. Pauca, J. Piper, and R. J. Plemmons, "Nonnegative matrix factorization for spectral data analysis," *Linear Algebra Appl.*, vol. 416, no. 1, pp. 29–47, 2006.
- [4] Y. T. Qian, S. Jia, J. Zhou, and A. Robles-Kelly, "Hyperspectral unmixing via $\ell_{1/2}$ sparsity-constrained non-negative matrix factorization," *IEEE Trans. Geosci. Remote Sens.*, vol. 49, no. 11, pp. 4282–4297, 2011.

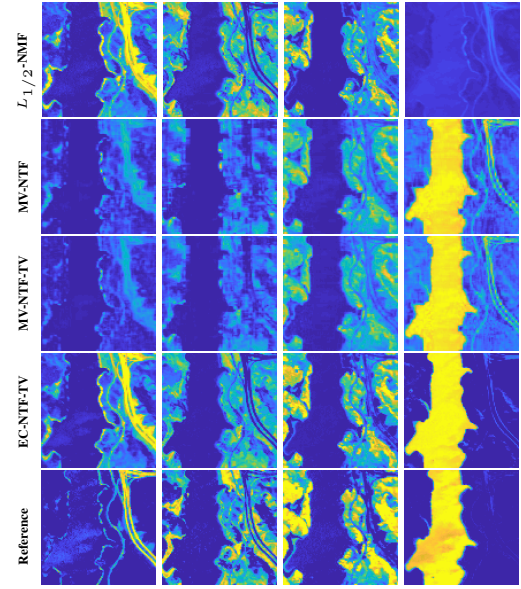


Fig. 4. References and estimated abundance maps by different unmixing algorithms for road, soil, tree, and water on Jasper Ridge data.

- [5] Y. Qian, F. Xiong, S. Zeng, J. Zhou, and Y. Tang, "Matrix-vector nonnegative tensor factorization for blind unmixing of hyperspectral imagery," *IEEE Trans. Geosci. Remote Sens.*, vol. 55, no. 3, pp. 1776–1792, 2017.
- [6] F. C. Xiong, Y. T. Qian, J. Zhou, and Y. Y. Tang, "Hyperspectral unmixing via total variation regularized non-negative tensor factorization," *IEEE Trans. Geosci. Remote Sens.*, vol. 57, no. 4, pp. 2341–2357, 2019.
- [7] T. G. Kolda and B. W. Bader, "Tensor decompositions and applications," *SIAM Rev.*, vol. 51, no. 3, pp. 455–500, 2009.
- [8] M. Iordache, J. M. Bioucas-Dias, and A. Plaza, "Collaborative sparse regression for hyperspectral unmixing," *IEEE Trans. Geosci. Remote Sens.*, vol. 52, no. 1, pp. 341–354, 2014.
- [9] S. Paris, P. Kornprobst, J. Tumblin, and F. Durand, "Bilateral filtering: Theory and applications," *Found. Trends Comput. Graph. Vis.*, vol. 4, no. 1, pp. 1–73, 2008.
- [10] D. D. Lee and H. S. Seung, "Algorithms for non-negative matrix factorization," in *Proc. 13th Int. Conf. Neural Inf. Process. Syst.*, 2000, pp. 556–562.
- [11] A. Beck and M. Teboulle, "Fast gradient-based algorithms for constrained total variation image denoising and deblurring problems," *IEEE Trans. Image Process.*, vol. 18, no. 11, pp. 2419–2434, 2009.